

## A bioenergetic mechanism for amoeboid-like cell motility profiles tested in a microfluidic electrotaxis assay

Hagit Peretz-Soroka\*, Reuven Tirosh, Jolly Hipolito, Erwin Huebner, Murray Alexander, Jason Fiege, Francis Lin\*

### Supplementary Information

#### Supplementary Figures and Movies Legends

**Figure S1. Microfluidic electrotaxis experiment setup and characterizations.** (A) The microfluidic device and experimental setup were modified from a previous system<sup>1</sup>. First, EF was applied to the microfluidic device using Ag/AgCl electrodes through agar salt bridges to prevent toxic products from the electrodes to contact with the cells. Ag/AgCl electrodes are preferred as they resist changes in pH. Electrotaxis experiment fails when the extracellular pH is below six<sup>2</sup>. Therefore, we worked with physiological buffer in order to preserve the physiological pH during our electrotaxis experiments. Second, we reduced the channel height to minimize flow and to allow the docking of cells. Third, the length of the small channel was adjusted to 1.5mm instead of 3mm. Fourth, EF was applied directly along the main center channel to improve EF and flow uniformity. These modifications improved the previous design for a higher throughput that the device was divided into four symmetric quarter regions. Each region was designed with several sub-zones to generate different EF simultaneously. Small channels and two symmetric inlets also served as medium control areas (R1 and R2). Fifth, we added a second PDMS layer on top of the medium reservoir inlets. Finally, we sealed the second layer with a cover glass to create a closed static environment, which minimized the flow; (B-D) We characterized the zone-dependent EF in the device by COMSOL simulation (B;D). In the current study we only selected the relatively uniform EF region, R3, as the observation field for electrotaxis experiments (C;D). Neutrophils isolated by negative selection were pre-activated by *f*MLP and then loaded into the microfluidic device (approximately  $1 \times 10^4$  cells for a final cell density of  $\sim 300$  cells/mm<sup>2</sup> attached to the channel). *f*MLP was washed away immediately before electrotaxis experiment.

**Figure S2. Characterizations of cell purity in the microfluidic device.** (A) DIC image of viable migrating neutrophils in all device zones; (B-D) Confocal images of neutrophil nucleus labeled with DAPI (blue) indicate > 98% of polymorphonuclear cells (B). Polymorphonuclear cell purity was further measured by granulocyte-specific activation antigen labeled by surface marker CD66 (green) on non-permeabilized cells for membrane CD66 (C) and on fixed permeabilized cells for cytoplasmic CD66 (D); (E) Intracellular granules of neutrophils were visible in the cytoplasm by Giemsa staining.

**Figure S3. Dose-dependent motility profiles of human neutrophils in *f*MLP concentration gradients.** The cell speed profiles in the *f*MLP gradient and in uniform *f*MLP field follow the same *f*MLP dose-dependency.

**Figure S4. Change of cell orientation in response to increasing EF.** (A) Electrotaxis experiments defined 3 sub-populations: cells that randomly migrated on the same spot before and during the application of an EF (red-3); cells that were not influenced by EF and continued to migrate toward the same direction (blue-1); cells that switched their directions before and during EF application (green-2); (B, D) Bar graphs represent percentage of cells that changed their original orientation in 2D under 2V/cm in phase 2 (B) and under 5V/cm in phase 3 (D); (C,E) Cell orientation change ( $\angle$ ) in increasing EF; (F) Angular velocity ( $\omega = \Delta\phi / \Delta t$  (degrees/sec)) per specific cell for increasing EF. The angle was measured manually using ImageJ.  $\phi_1$  = Cell angle in the last frame of control conditions (0V/cm) before EF was applied.  $\phi_2$  = Cell angle in the first frame as soon as cell orientation becomes stable under EF (Note: this is not the first frame after EF was applied). Analysis was done for human neutrophil subpopulations and labeled as described in Figure 4. Pie chart colors in (C, E) indicate the percentage of subpopulation as labeled in the X axis.

**Figure S5. When the EF direction was switched, cells that were moving in the field direction (close to 0° or 180°) will change their electric dipole orientation slowly.** In the iPC-CS model, this observation can be considered to result from a nearly zero torque by the EF. Blue: No EF; Red: EF direction to the right; Black: EF direction to the left.

**Movie 1.** Animation of the iPC-CS model.

**Movie 2.** Amoeboid-like movement and fountain-like streaming of a representative human neutrophil.

**Movie 3.** Human neutrophil movement in phase 1 under increasing EF up to ~10V/cm over 35min.

**Movie 4.** Representative human neutrophil movement in the 3 phases.

**Movie 5.** High magnification imaging of human neutrophil migration toward the cathode under low EF.

**Movie 6.** High magnification imaging of human neutrophil migration toward the anode under high EF.

**Movie 7.** Low magnification imaging of human neutrophil migration toward the cathode under increasing EF.

**Movie 8.** Random migration of human neutrophils in the absence of EF.

**Movie 9.** Low magnification imaging of human neutrophil bidirectional migration under increasing EF.

## Supplementary Figures

Figure S1

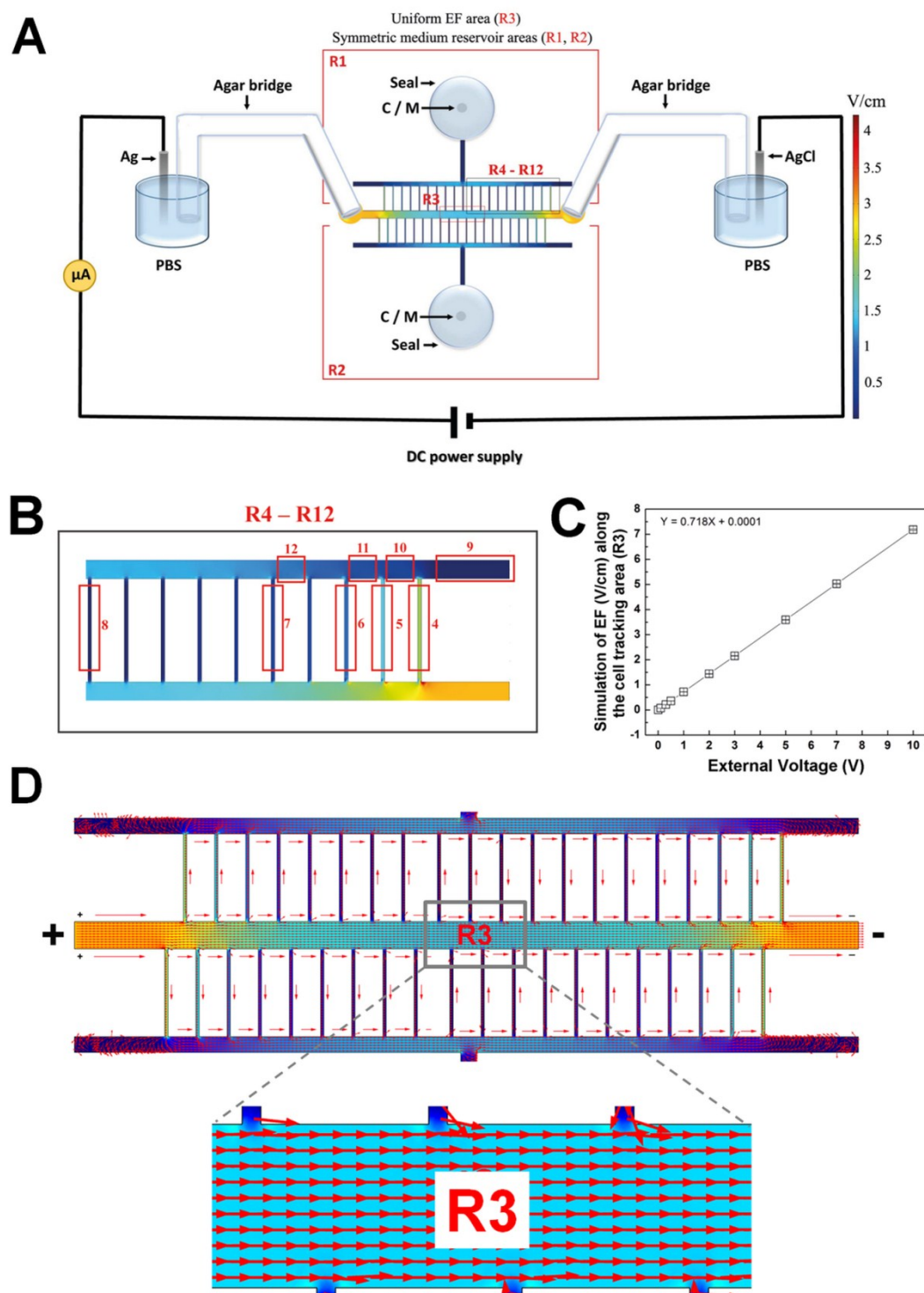


**Figure S2**

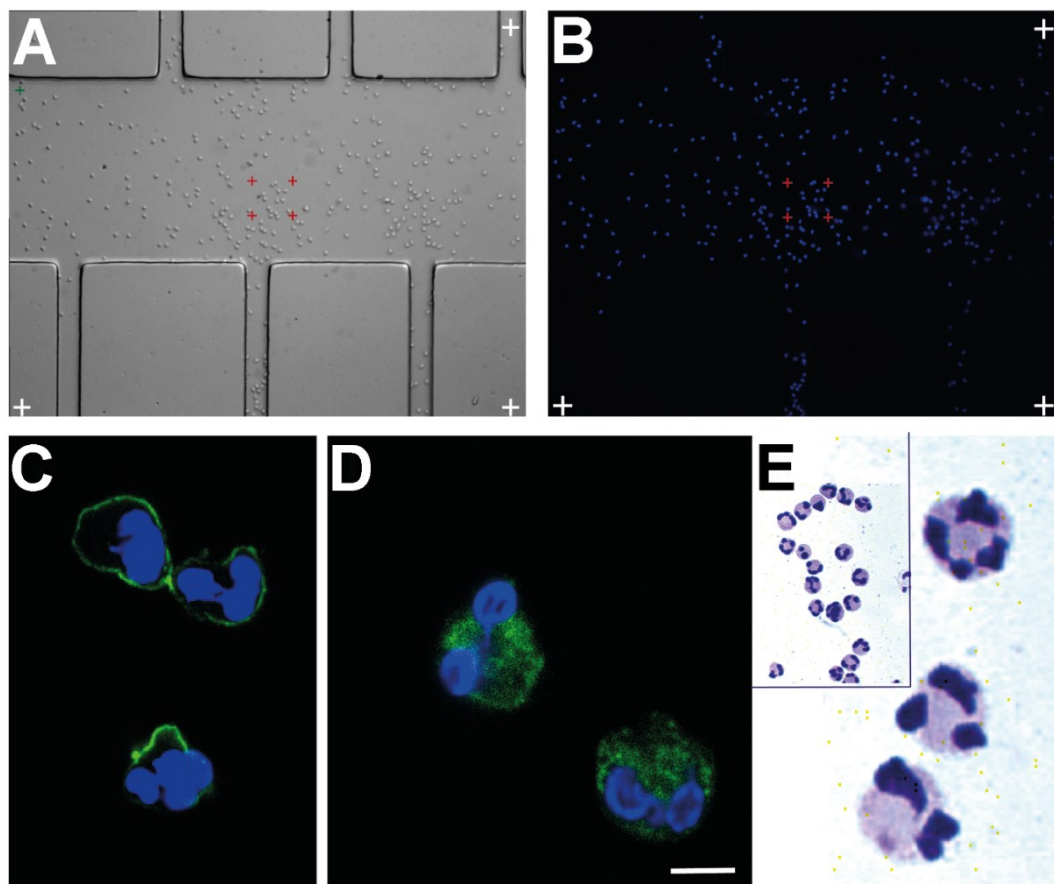


**Figure S3**

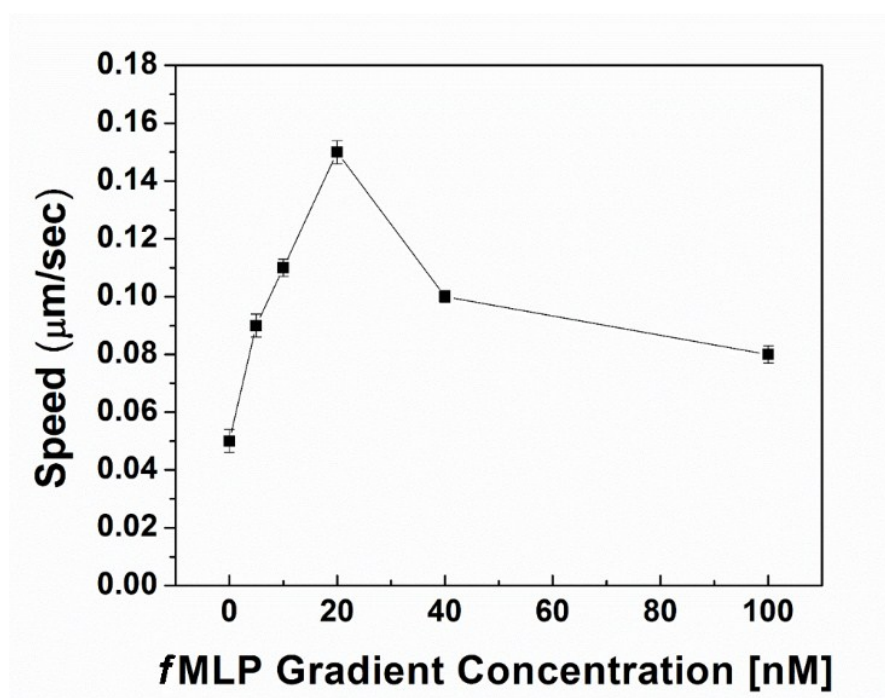
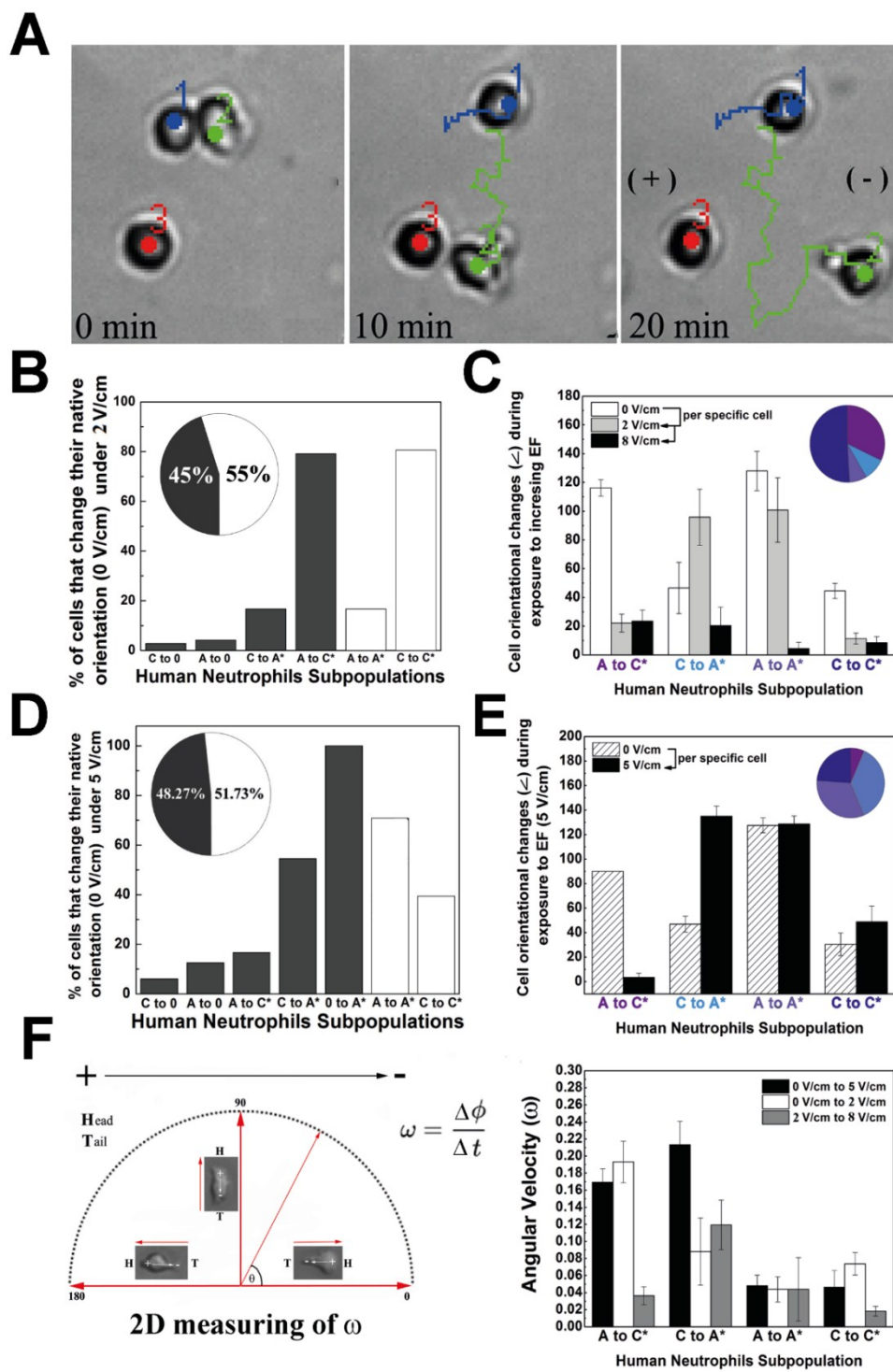
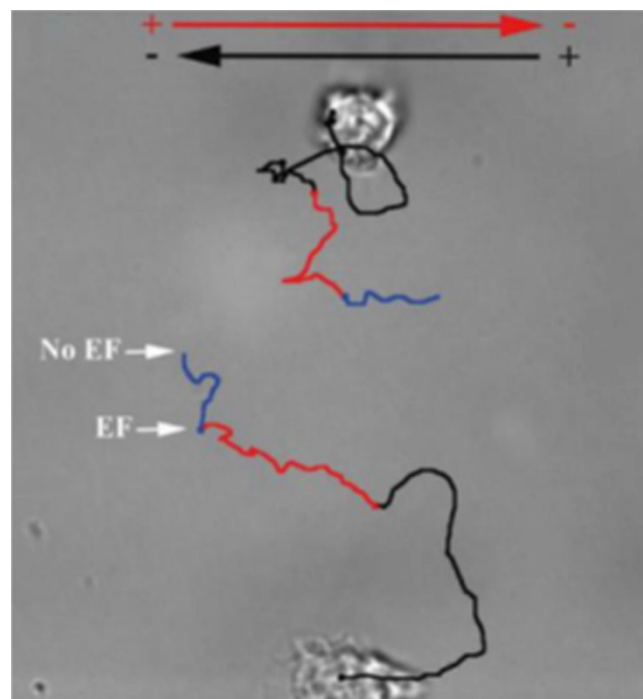


Figure S4



**Figure S5**



## References

1. J. Li, L. Zhu, M. Zhang and F. Lin, *Biomicrofluidics*, 2012, **6**, 024121.
2. G. M. Allen, A. Mogilner and J. A. Theriot, *Current Biology*, 2013, **23**, 560-568.